

SCIENTIFIC REPORTS



OPEN

Bulk and surface recombination properties in thin film semiconductors with different surface treatments from time-resolved photoluminescence measurements

Received: 10 October 2018

Accepted: 14 March 2019

Published online: 29 March 2019

Thomas P. Weiss^{1,2}, Benjamin Bissig¹, Thomas Feurer¹, Romain Carron¹, Stephan Buecheler¹ & Ayodhya N. Tiwari¹

The knowledge of minority carrier lifetime of a semiconductor is important for the assessment of its quality and design of electronic devices. Time-resolved photoluminescence (TRPL) measurements offer the possibility to extract effective lifetimes in the nanosecond range. However, it is difficult to discriminate between surface and bulk recombination and consequently the bulk properties of the semiconductor cannot be estimated reliably. Here we present an approach to constrain systematically the bulk and surface recombination parameters in semiconducting layers and reduces to finding the roots of a mathematical function. This method disentangles the bulk and surface recombination based on TRPL decay times of samples with different surface preparations. The technique is exemplarily applied to a CuInSe₂ and a back-graded Cu(In,Ga)Se₂ compound semiconductor, and upper and lower bounds for the recombination parameters and the mobility are obtained. Sets of calculated parameters are extracted and used as input for simulations of photoluminescence transients, yielding a good match to experimental data and validating the effectiveness of the methodology. A script for the simulation of TRPL transients is provided.

Minority carrier lifetime τ is generally evaluated by using time-resolved photoluminescence (TRPL) in thin film semiconductors, such as Cu(In,Ga)Se₂ (CIGS)^{1–5}, CdTe⁶ or perovskite^{7–10}. However, these photo luminescence (PL) decay times are influenced by surface recombination and hence do not yield the bulk lifetime, which is a desired value indicating the quality of the semiconductor under test. A straightforward extraction of the bulk lifetime from the measured decay of the PL signal is generally not possible since various recombination channels happen simultaneously and are also influenced by diffusion processes¹¹. An interpretation of the TRPL decay time as the bulk lifetime leads in turn to an underestimation, which might result in incorrect conclusions. Fitting approaches are also not well suited as several sets of parameters can generally very well reproduce the experimental transients. Several methods were proposed to decouple the effects of diffusion and surface recombination from the bulk recombination. Transient reflectance spectroscopy was proposed to measure the surface recombination as well as the diffusion into the bulk on perovskite single crystals¹² but can only be applied to free surfaces. On the other hand, passivated surfaces are required to stabilize the interface properties and cannot be measured with the method proposed in¹². The extraction of charge carriers facilitated by hole or electron transporting layers has also been used as a measure for the bulk lifetime and diffusion coefficient of perovskite absorber layers^{9,10}. In that case

¹Laboratory for Thin Films and Photovoltaics, Empa–Swiss Federal Laboratories for Materials Science and Technology, Überlandstrasse 129, 8600, Dübendorf, Switzerland. ²Present address: Laboratory for Photovoltaics, Physics and Materials Science Research Unit, University of Luxembourg, L-4422, Belvaux, Luxembourg. Thomas P. Weiss and Benjamin Bissig contributed equally. Correspondence and requests for materials should be addressed to T.P.W. (email: thomas.weiss@uni.lu)

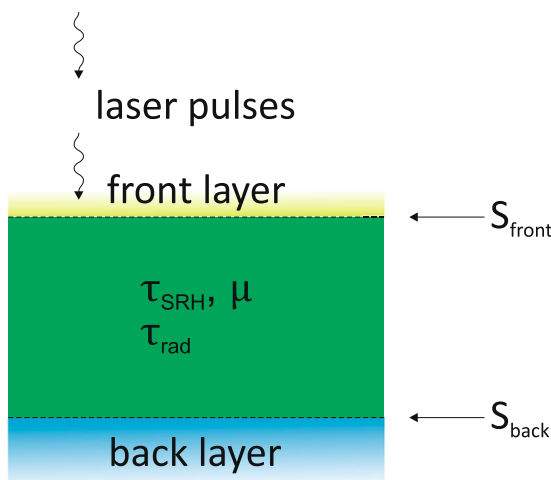


Figure 1. Model for the TRPL interpretation. Parameters describing non radiative recombination are the surface recombination velocities at the front and back side of the absorbers S_{front} and S_{back} as well as the bulk lifetime τ_{SRH} and mobility μ of the CIGS absorber. The radiative recombination is taking into account with $\tau_{rad} = 1.7 \mu s$.

however, the drift of charge carriers¹³ due to a built-in electric field was not taken into account, leading to an underestimated bulk lifetime and an overestimated diffusion coefficient.

Another method was proposed by Barnard *et al.*¹⁴ and Kuciauskas *et al.*¹⁵ that is based on two-photon excited TRPL. With this method carriers are excited deeper inside the bulk of the semiconductor, which decreases the influence of the front surface recombination on the initial decay characteristics of the PL signal^{14,15}. Still, the mono-exponential tail decay time only corresponds to an effective lifetime governed by bulk- and surface recombination and not the bulk lifetime of the semiconductor¹⁵.

Ahrenkiel and Johnston proposed an approach based on resonant-coupled photoconductive decay data in the microsecond range to determine the surface recombination velocity and diffusion constant for Si wafers¹⁶. A multi-dimensional least square fit is applied to discriminate the obtained parameters. Hempel *et al.*¹⁷ followed a similar approach by using terahertz spectroscopy, which allows a resolution of 0.1 ps and therefore enables the fitting of the initial decay curve and thus the surface recombination velocity for thin films with carrier dynamics in the sub nanosecond range. However, this methodology cannot be adapted to TRPL data due to a limited temporal resolution¹⁷. In particular, we show by simulations that a large range of parameters can describe reasonably well the PL decay curves, which limits the use of such a fitting approach.

Staub *et al.* determined an upper limit of the surface recombination velocity assuming that the non-radiative lifetime is solely caused by interface recombination⁷. This approach might be useful for high PL decay times observed for instance in high quality perovskite layers⁷, however, might not yield reasonable limits for other thin film technologies with lower effective lifetimes.

In this paper we present a technique based on the mathematical treatment of PL decay times acquired from compound semiconducting layers with different front and back surface modifications. A model involving surface and Shockley-Read-Hall (SRH) recombination as well as diffusion of excited charge carriers is applied to discriminate these recombination channels. The analysis is carried out on CuInSe₂ (CIS) and single back-graded Cu(In,Ga)Se₂ (bg-CIGS) layers used in solar cells¹⁸ with various surface modifications. These materials were chosen due to their complexity and the possibility to introduce a bandgap grading throughout the semiconducting layer. However, the approach can be applied to other semiconducting material systems as well. Based on the model, upper and lower bounds for the surface recombination velocities are extracted as well as estimates for the bulk properties such as the minority carrier mobility and bulk lifetime. A Matlab script is used to simulate transients based on possible sets of parameters, which reproduce the experimental transients. The source code of this script is available in the Supplementary Information.

The manuscript is structured as follows: section 2 introduces the theoretical background for the analysis of the TRPL decay time based on bulk and surface recombination contributions. Section 3 describes the experimental details for the measurement of TRPL transients as well as the sample preparation. The analysis of the decay times and the discussion of material and interface parameters are given in section 4. Simulated transients using sets of parameters extracted from the mathematical methodology are presented in section 5. The range of valid values for all parameters involved in the underlying model is discussed.

Theoretical background

Device model and mathematical solution for a TRPL transient. In order to analyze the PL transients the model shown in Fig. 1 is used. It assumes an absorber layer with a homogeneous non-radiative bulk lifetime τ_{SRH} and mobility μ . In particular, the electron and hole mobilities μ are assumed to be equal and hence no ambipolar transport is considered. Thus, in low injection conditions (as realized in the experiments in the present paper), the minority carrier lifetime is probed, while in high injection conditions the smaller mobility of the two

Description	Notation	Unit	Value
rad. rec. coefficient	B	$cm^3 s^{-1}$	1.67×10^{-10}
absorption coefficient	α	μm^{-1}	8.12
absorber doping	p_0	cm^{-3}	3.5×10^{15}
absorber thickness	d	μm	3.0
eff. density of states	N_e, N_v	cm^{-3}	2×10^{18}
temperature	T	K	300

Table 1. Parameters used for simulating PL transients.

charge carriers is probed¹⁹. Also τ_{SRH} is equal for electrons and holes, which can be realized by midgap defect states according to $\tau_{SRH} = 1/v_{th}\sigma N_t$ (under low injection conditions²⁰), where v_{th} is the thermal velocity of free charge carriers, σ the capture cross section for electrons and holes of the midgap defect state and N_t its total density. In addition, surface recombination at the front and back side of the absorber is included and is described by the recombination velocities S_{front} and S_{back} , respectively.

The radiative recombination rate R_{rad} is described by

$$R_{rad} = B((n_0 + \Delta n)(p_0 + \Delta n) - n_0 p_0) \quad (1)$$

The equilibrium densities for electrons and holes are denoted by n_0 and p_0 , respectively and the excess electron and hole density by Δn . For a p-type semiconductor ($p_0 \gg n_0$) and under low injection conditions ($p_0 \gg \Delta n$), Eqn. (1) reduces to

$$R_{rad} = B p_0 \Delta n = \frac{\Delta n}{\tau_{rad}} \quad (2)$$

with the radiative lifetime $\tau_{rad} = 1/B p_0$ ²¹. For Eqn. (2) it is assumed that $\Delta n = \Delta p$, i.e. without trapping and charge carrier separation. The radiative recombination constant B is taken from ref.²⁰ and is set to $1.67 \times 10^{-10} cm^3 s^{-1}$ (see also Table 1). Capacitance voltage measurements were applied to determine $p_0 = 3.5 \times 10^{15} cm^{-3}$ (see Supplementary Information B for more details). Thus, the radiative lifetime evaluates to $\tau_{rad} \approx 1.7 \mu s$ and is kept constant in this study.

Mathematical solution. For a mathematical solution of the PL transient the continuity Eqn. (3) including drift and recombination needs to be solved.

$$\frac{\partial \Delta n}{\partial t} = -R_{rad} - R_{SRH} + \frac{\mu k T}{q} \frac{\partial^2 \Delta n}{\partial z^2} + g \quad (3)$$

where g denotes the generation profile of the laser pulse (see Eqn. (13)). In the following, the pulse is assumed infinitesimal short, i.e. $exc(t) = \delta(t)$ with n_γ the number of photons per pulse and area. Solutions for other pulse profiles can then be obtained by convolution¹¹. Using low injection conditions for the radiative and SRH recombination rate R_{rad} and R_{SRH} , Eqn. (3) reads

$$\frac{\partial \Delta n}{\partial t} = -\Delta n \left(\frac{1}{\tau_{rad}} + \frac{1}{\tau_{SRH}} \right) + \frac{\mu k T}{q} \frac{\partial^2 \Delta n}{\partial z^2} \quad (4)$$

The solution for Eqn. (3) was calculated (without τ_{rad}) using the surface recombination velocities S_{front} and S_{back} as boundary conditions^{11,22}. The solution (including τ_{rad} in this case) reads^{11,22,23}:

$$\Delta n(t, z) = A_0 + \sum_{k=1}^{\infty} A_k U_k(z) \exp(-\eta_k t) \quad (5)$$

with

$$\eta_k = \frac{1}{\tau_{rad}} + \frac{1}{\tau_{SRH}} + D \beta_k^2 \quad (6)$$

and

$$\tan \beta_k d = - \frac{D(S_{back} + S_{front}) \beta_k}{S_{back} S_{front} - D^2 \beta_k^2} \quad (7)$$

Here $D = \mu k T / q$ denotes the diffusion constant and d the thickness of the semiconductor layer. The functions $U_k(z)$ and prefactors A_k are dependent of the surface recombination and are given by^{11,23}

$$U_k(z) = \cos\beta_k z + \frac{S_f}{D\beta_k} \sin\beta_k z \quad (8)$$

$$A_k = \alpha n_\gamma \frac{\int_0^d dz \exp - \alpha z U_k(z)}{\int_0^d dz U_k^2(z)} \quad (9)$$

Equation(7) is solved numerically for β_k with $0 < \beta_1 < \beta_2 < \dots$. As the β_k coefficients are strictly increasing with k , the contribution to $\Delta n(t, z)$ of the summed terms at later times is decreasing exponentially due to the term $\exp(-\eta_k^2 t)$ in Eqn. (5). Consequently, the decay at long times of a measured transient can be described by using only the first term with $k = 1$, which describes the recombination at the surfaces and in the bulk^{11,24}. Note that $A_0 = 0$ if either of the surface recombination velocities is non-zero²³. Consequently, at late times Eqn. (5) reduces to

$$\Delta n(t, z) = A_1 U_1(z) \exp \left(- \left[\frac{1}{\tau_{rad}} + \frac{1}{\tau_{SRH}} + D\beta_1^2 \right] t \right) \quad (10)$$

Late times refers to the time until the injected carriers diffused into the semiconducting layer and are in quasi equilibrium, i.e. the surface recombination constant is not dependent on time anymore. Maiberg *et al.* showed that diffusion takes place within a few ns for a mobility $> 10 \text{ cm}^2 \text{V}^{-1} \text{s}^{-1}$ and a layer thickness of $3 \mu\text{m}$. Experimentally, this can be observed by a single exponential decay.

As A_1 and $U_1(z)$ are time independent in Eqn. (10), the effective lifetime τ_{eff} can be written as

$$\frac{1}{\tau_{eff}} = \frac{1}{\tau_{rad}} + \frac{1}{\tau_{SRH}} + \frac{1}{\tau_{surf}} \quad (11)$$

with

$$\frac{1}{\tau_{surf}} = D\beta_1^2 \quad (12)$$

It is stressed that the surface term τ_{surf} includes the surface recombination at the front- and the backside via Eqn. (7) as well as the mobility, which is included in the diffusion constant. Therefore the effective tail decay time τ_{eff} can be expressed as a function of 4 free parameters: S_{front} , S_{back} , μ , τ_{SRH} .

In section 4 the expression (11) is used to calculate the effective lifetime based on these four parameters. Then the comparison to experimental PL decay times allows deducing boundary values for these 4 parameters. It is pointed out that good analytical approximations for Eqn. (7) exist in the two special cases: $S_{front} = S_{back} = S$ or that either of the recombination velocities is zero^{11,22}. However, in the general case of $S_{back} \neq S_{front} \neq 0$, which is used in the present paper, Eqn.(7) needs to be solved numerically.

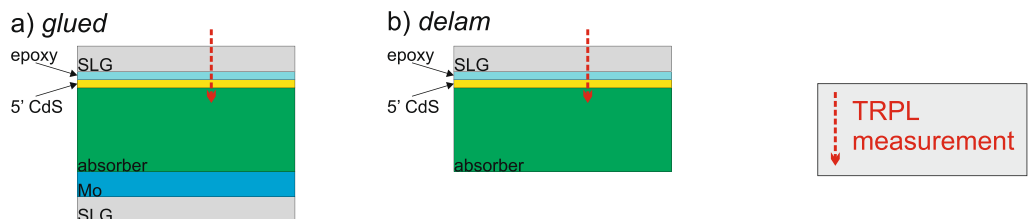
Recently, trapping of minority carriers has also been proposed to influence the measured decay tail time^{25–27}, which was mainly motivated by a strong temperature dependence of the decay tail time²⁶. While trapping was included into the model presented in²⁷, no temperature dependent transients were measured. Redinger *et al.* measured temperature dependent transients in air and in N_2 environment and showed that the strong temperature dependence can result from a degradation of the front surface²⁸. For the CIS and the bg-CIGS absorbers investigated in this study the TRPL curves do not show a strong temperature dependence and thus might be explained solely by the temperature dependence of the Shockley-Read-Hall recombination rate (see Supplementary Fig. 3). It is noted that this argument alone is not sufficient to exclude an influence of trapping. However, due to simplicity, trapping is not included in the analysis presented in this paper.

Simulations of time-resolved photoluminescence transients. If not mentioned otherwise, 1D simulations of PL transients were carried out using a Matlab script, which is provided in the supporting information. The script solves the drift-diffusion equation as well as the continuity equation for electrons and holes. Bulk defects are implemented using SRH statistics and surface recombination by surface recombination velocities. The Poisson equation is not solved and hence ambipolar transport is not taken into account. Further details concerning the physics of the Matlab script are given in Supplementary Information A.

The conduction band grading for one of the semiconductor under test (see section 3.2) is implemented on each mesh point by a potential energy for the electrons. Material parameters used for the simulations are listed in Table 1. Other parameters, such as bulk lifetime, surface recombination velocities and mobilities are estimated and discussed in the main text.

In order to verify the results obtained by the Matlab script a number of transients with relevant parameter variations were simulated using Sentaurus TCAD, see supporting information A. For TCAD simulations the graded conduction band was implemented by splitting the semiconductor region into 40 sub-regions and by linearly interpolation between these regions subsequently.

Back surface modifications



Front surface modifications

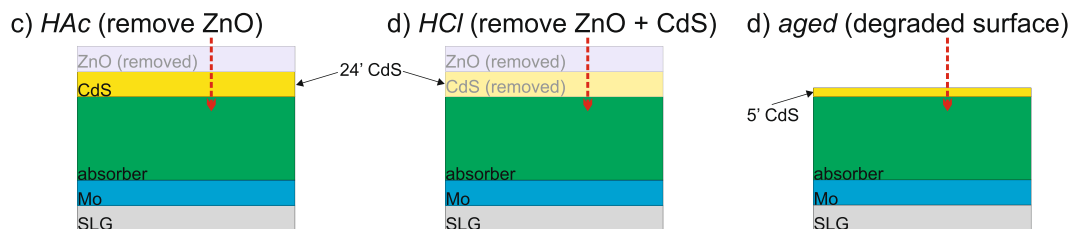


Figure 2. Sample modifications for measuring the same absorber with different surface conditions.

Optical generation. Experimentally, free electron-hole pairs are generated by a pulsed laser, as described in the experimental section 3.1. For the simulations the absorption and hence the generation is described by Beer-Lambert law according to

$$g(z, t) \propto n_\gamma \text{exc}(t) \alpha \exp(-\alpha z) \quad (13)$$

with the absorption coefficient $\alpha = 8.12 \mu\text{m}^{-1}$ at 639 nm, which was determined by in-house measurements of CIS layers²⁹. The normalized function $\text{exc}(t)$ describes the shape of the laser pulse, which is used for simulated transients (section 5), and the α factor normalizes the exponential term. The total number of injected electron-hole pairs per pulse and per area n_γ is estimated from the laser power and excitation spot area.

Experimental

TRPL measurements. For TRPL measurements the sample is excited with a 639 nm laser on a spot of roughly $50 \mu\text{m}$ diameter with a pulse FWHM of around 100 ps. The PL emission is collected by an optical system with numerical aperture of 0.22 and detected by a Peltier cooled InGaAs photomultiplier tube. A monochromator in the detection chain is set to 0th order, i.e. the PL transients were spectrally integrated. The excitation density was estimated by measuring the current of a Si reference cell for the different laser intensity settings used in this study.

Sample preparation. The samples were grown on Mo coated glass substrates by a multistage co-evaporation process as described in ref.¹⁸ (samples CIS and BG2 therein). For the CuInSe₂ (CIS) sample only In was supplied as a group-III element during the growth, resulting in a constant bandgap through the depth of the absorber. For the single graded Cu(In,Ga)Se₂ (bg-CIGS) sample, Ga was supplied within the first stage of the deposition process, realizing a Ga gradient only towards the back contact. The front side of the bg-CIGS layer has a bandgap of around 1 eV similar to the pure CuInSe₂ absorber and hence similar absorption characteristics¹⁸. The [Ga]/([Ga] + [In]) (GGI) grading profile as measured by secondary ion mass spectrometry (SIMS) of the bg-CIGS absorber investigated here is shown in Supplementary Fig. 1. (black line). The layer shows a GGI at the back of 0.28. For simulated transients the GGI grading is implemented as a conduction band grading as detailed in section 2.2. Parts of the absorber layers were completed into solar cell devices with a stack of CdS/ZnO/Al:ZnO and a Ni/Al grid (see ref.¹⁸ for details).

TRPL measurements were carried out on the absorbers with various surface treatments, and not on full devices to exclude severe charge separation effects³⁰. These surface treatments were applied to modify the front or the back surface of the absorber and consequently the surface recombination velocities. Figure 2 displays the various configurations and modifications for the front and back surfaces. These configurations can be described as follows:

- i. *glued*: a thin CdS layer was grown by a 5 minute chemical bath deposition (CBD) process to stabilize and passivate the front surface of the absorber layer^{31,32}. The deposition time was kept short to limit the CdS thickness and to avoid the formation of an electric field due to the formation of a pn junction³³ (see also the configuration *HAc*). After CdS deposition a glass substrate was glued on top with an approximately $30 \mu\text{m}$ thick transparent epoxy layer. It was checked that the epoxy layer does not emit parasitic luminescence during a TRPL measurement. For this configuration the absorber back surface remains in contact to the Mo/glass substrate.

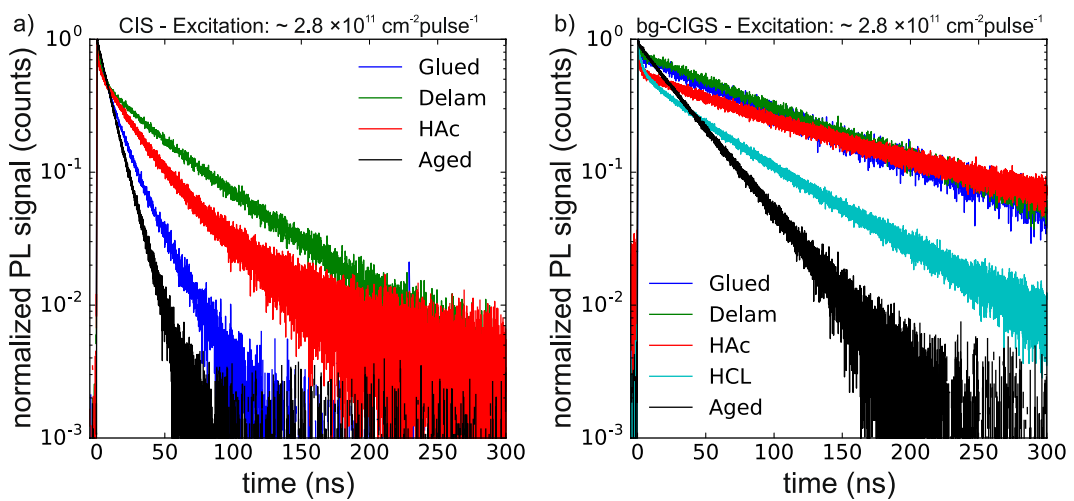


Figure 3. Normalized PL transients of the CIS and the back graded CIGS absorber. Various surface modifications are applied demonstrating the effect of the surface recombination velocity.

- ii. *delam*: The sample is prepared as described for the *glued* configuration. However, the sample is subsequently detached from the Mo/glass substrate. The back side of the absorber is not in contact to the Mo layer anymore, but exposed to air.
- iii. *HAc*: Starting from a finished device the ZnO was removed by 1 min etching (sonication) in 5% acetic acid (HAc) leaving only approximately 50 nm (24 min CBD) of CdS (see Supplementary Fig. 2). The back side of the absorber is in contact to the Mo/glass substrate. It is noted that TRPL measurements of the device after removal of the window layer are very similar to those of an absorber directly after the deposition of a thick CdS layer (not shown).
- iv. *HCl*: Starting from a finished device the ZnO and the CdS layers were removed by 1 min etching (sonication) in 5% hydrochloric acid (HCl) leaving the bare absorber surface exposed (see Supplementary Fig. 2). The back surface is in contact to the Mo/glass substrate. For the CIS sample the HCl etch led to uncontrolled flaking of the absorber. Thus, this configuration could only be applied for the bg-CIGS absorber.
- v. *aged*: same as i) but without gluing a glass substrate onto the front side. The sample with a thin CdS layer did not show any degradation in a TRPL measurement within a few days. However, after storing the sample in ambient conditions for approximately 3 months a degradation was observed in terms of a faster PL decay. In the subsequent analysis the configuration *aged* denotes the condition after the 3 months storage. It is noted that the configuration *glued* did not show any signs of degradation.

Results and Discussion

Figure 3 shows normalized PL transients measured on the CIS and the bg-CIGS absorber for the surface modifications described in section 3.2. In general, the transients show a small initial non-exponential decay (during the first few ns after the excitation) and a single-exponential decay after approximately 20 ns. The focus of the subsequent analysis is the single-exponential decay at late times (after 20 ns). In this regime it is assumed that the system can be described by low injection conditions and that the PL decay time can be described by Eqn. (11), i.e. by a single exponential decay with effective lifetime τ_{eff} . Low injection conditions in this regime are indicated by the single exponential behavior. In addition, assuming that the carriers have homogenized in the $3 \mu m$ thick absorber (in the single exponential region) results in an excess carrier density of $2.8 \times 10^{11} cm^{-2}/3 \mu m \approx 1 \times 10^{15} cm^{-3}$, which is below the doping density of $3.5 \times 10^{15} cm^{-3}$. In the following sections the lifetimes were extracted consistently between 20 ns and 80 ns to prevent any influence of possible high-injection conditions and residual background. As the modification of the surfaces is not expected to influence the bulk properties, the changes in the decay time for different sample configurations can be assigned to the front and back surface recombination terms given by $\tau_{surf}^{-1} = D\beta_s^2$. In the following, the results obtained for the CIS (section 4.1) and the bg-CIGS (section 4.2) absorbers are investigated separately. Subsequently, the obtained recombination parameters are discussed in section 4.3 and compared to simulated transients (section 5).

Surface recombination analysis for the CIS absorber. Table 2 reports the experimental decay times, which span from 11 ns (*aged*) to 48 ns (*delam*) for the CIS absorber. An important observation is that the decay time in the *delam* configuration is strongly increased compared to the *glued* configuration (see also Fig. 3a, green and blue curve, respectively). The only difference is the back contact and hence the back surface recombination, which for the *glued* configuration (in contact with the Mo/glass substrate) is much stronger. For the following analysis, the surface recombination velocity of the CIS/Mo interface is set to $S_{back,Mo} = 1 \times 10^6 cm s^{-1}$ (see Supplementary Information

Measured decay times in ns					
	glued	delam	HAc	HCl	aged
CIS	17	48	30	—	11
bg-CIGS	98	105	118	57	34

Table 2. Decay times of measured PL decay curves shown in Fig. 3. The decay times were extracted from a single exponential fit in the range 20 ns to 80 ns.

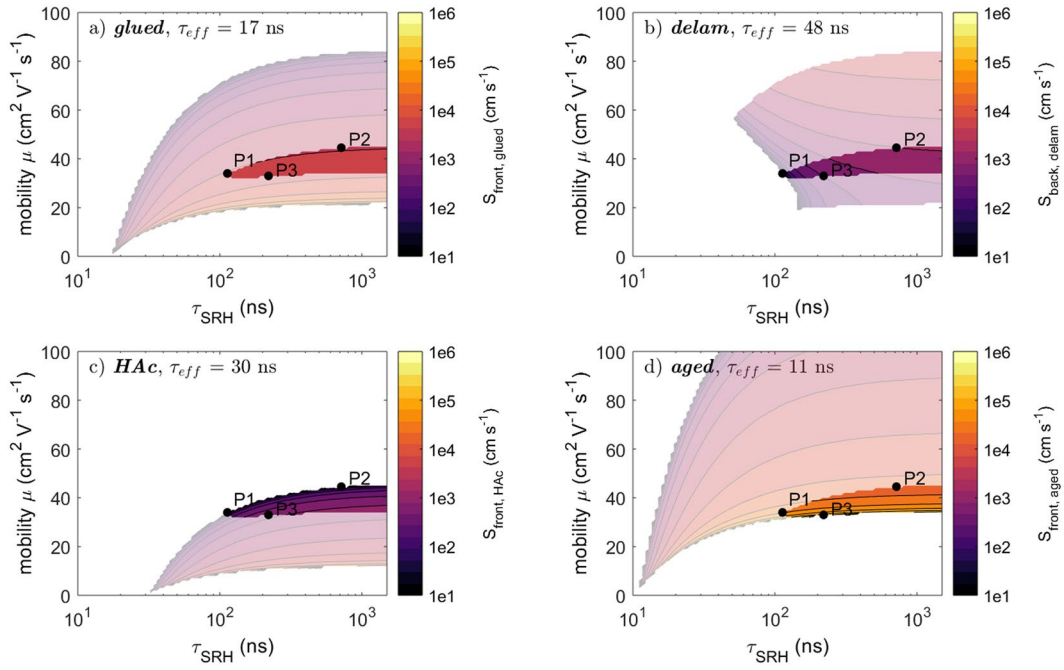


Figure 4. Estimation of the valid parameter values of τ_{SRH} , μ and the unknown surface recombination velocity of the corresponding sample configuration according to Eqn. (14) for the CIS absorber. The pale color maps in the background indicate the parameters satisfying Eqn. (14) when only a single measurement for the indicated configuration is taken into account. The bright (and smaller) color map is the intersection of all individual color maps. These bright maps take also the restrictions for τ_{SRH} and μ into account, which are given by the measurements of the other configurations.

B for further discussion). It is noted that similar results are obtained with a weaker $S_{back,Mo} = 1 \times 10^5 \text{ cms}^{-1}$ and a stronger $S_{back,Mo} = 1 \times 10^7 \text{ cms}^{-1}$ back surface recombination velocity (not shown).

In the following, a systematic approach is described to confine the value range of the remaining parameters based only on the effective decay times presented in Table 2. As discussed in section 2.1.1 each of these effective decay times is determined by a set of parameters $(\tau_{bulk}, \mu, S_{front}, S_{back})$ through Eqn. (11).

To explore the parameter space a numerical solution has been calculated to the equation

$$\tau_{exp,i} = \tau_{eff}(\tau_{bulk}, \mu, S_{front,i}, S_{back,i}) \quad (14)$$

where $\tau_{exp,i}$ denotes the experimentally measured lifetime for the configuration i (glued, delam, HAc, aged) reported in Table 2. For the configurations in contact with the Mo substrate the back surface recombination velocity was set to the fixed value $S_{back,Mo} = 1 \times 10^6 \text{ cms}^{-1}$ as described above. For the delam configuration the front surface is the same as for the glued configuration and therefore $S_{front,delam} = S_{front,glued}$. Consequently, for each configuration the parameter space to Eqn. (14) is reduced down to 3 free variables. By imposing values to the (τ_{bulk}, μ) parameters, a solution may be found for the surface recombination velocity such that Eqn. (14) is fulfilled. Figure 4 presents the solutions to the surface recombination velocity as a function of the two absorber parameters τ_{bulk} and μ , for each sample configuration. A white background indicates that no solution exists for that particular combination of (τ_{bulk}, μ) . The pale colors represent combinations of (τ_{bulk}, μ) were solutions were found based on Eqn. (14), for each configuration separately. Thus, each configuration results in different restrictions to the parameter space. As the same absorber is used for all surface configurations, the values for τ_{bulk} and μ are expected to be the same and independent of the surface configuration. Therefore, valid (τ_{bulk}, μ) values must allow solutions for each and every sample configuration. These regions are obtained by the intersection of the valid parameter space of each individual configuration and are displayed as bright regions in Fig. 4. These maps show that the parameters governing the recombination can effectively be confined by measurements on different

		CIS		bg-CIGS	
		lower limit	upper limit	lower limit	upper limit
$S_{front, glued}$	cms^{-1}	5.3×10^3	9.1×10^3	3.0×10^2	1.8×10^3
$S_{front, HAc}$	cms^{-1}	0	1.4×10^3	4.4×10^1	1.4×10^3
$S_{front, aged}$	cms^{-1}	2.2×10^4	∞	3.2×10^3	∞
$S_{front, HCl}$	cms^{-1}	n/a		1.4×10^3	4.7×10^3
$S_{back, delam}$	cms^{-1}	0	1.9×10^3	n/a	
τ_{bulk}	ns	117	∞	132	∞
μ	$cm^2V^{-1}s^{-1}$	32	45	8.3	∞ (*)

Table 3. Boundary values for the surface recombination velocities and the absorber properties based on the mathematical analysis presented in sections 4.1 (CIS) and 4.2 (bg-CIGS). For the calculations of the CIS absorber a surface recombination velocity at the Mo interface was chosen to be $S_{back, Mo} = 10^6 cms^{-1}$.
(*) Simulations of transients could provide an upper limit to the mobility μ in the bg-CIGS absorber.

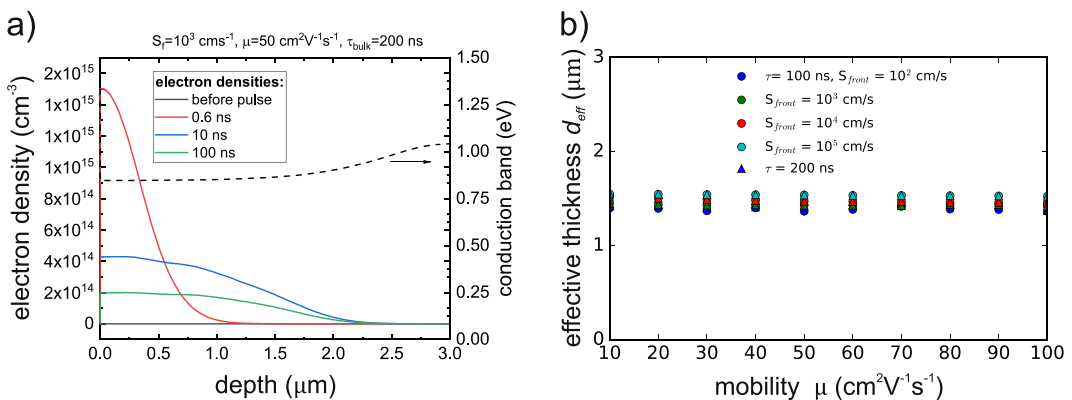


Figure 5. (a) TCAD simulations of the electron density within the back graded absorber bg-CIGS for different times after the excitation pulse. The back grading results in a decreased electron density towards the back confining the electrons within an effective depth d_{eff} . (b) Calculated effective thickness for the back graded CIGS absorber according to Equations (7) and (11) with the same parameters τ_{bulk} , S_{front} , μ as used by the TCAD simulations.

sample configurations (*glued*, *delam*, *HAc*, *aged*). Boundary values for each recombination parameter are then extracted by minimum and maximum value in each (intersected) map and are listed in Table 3. The mobility is confined between 32 and $45 cm^2V^{-1}s^{-1}$ and the bulk lifetime takes values above $117 ns$. This value is significantly larger than the highest measured decay time ($48 ns$ for the *delam* configuration) and shows a clear influence of the surface recombination on experimental data.

In section 4.3 three parameter sets P1, P2 and P3 obtained from this approach will be used as input for simulated transients. It will be shown that the parameters indeed result in correct decay times and can describe the experimental transients with a reasonable match.

Surface recombination analysis for the bg-CIGS absorber. Figure 3b shows the experimental transients for the configurations used for the bg-CIGS absorber and Table 2 reports the extracted decay times. Compared to the CIS absorber the transients for the *glued* and the *delam* configuration are very similar, demonstrating that the Ga back grading (increase of GGI by 0.28) efficiently prevents the recombination at the back contact. Simulations support this assumption (presented in Supplementary Fig. 4), which show that a conduction band increase of $193 meV$ towards the back contact (equivalent to a GGI at the back contact of 0.28) yields transients independent of the back surface recombination velocity. The recombination at the back contact is prevented by a very low electron density in this high bandgap region, while the electrons are concentrated in the low bandgap region (Fig. 5a). This effect is accounted for in the solution of Eqn. (11) by modeling the bg-CIGS absorber as an ungraded layer with a thinner effective thickness d_{eff} and a low back surface recombination velocity. In order to set a reasonable d_{eff} value, TCAD transients were simulated implementing the grading shown in Supplementary Fig. 1 using a few sets of input parameters S_{front} , S_{back} , μ , τ_{bulk} . The simulated decay times were used in the model of Eqn. (11): by imposing the same S_{front} , μ , τ_{bulk} parameters and $S_{back} = 0 cms^{-1}$ a solution of the effective thickness d_{eff} is calculated and presented in Fig. 5a. The solution of d_{eff} is consistently between 1.4 and $1.6 \mu m$ and matches roughly the absorber depth, where the increase in the conduction band corresponds to the thermal energy $k_b T$. Thus, for the ongoing analysis of the bg-CIGS absorber a value of $d_{eff} = 1.5 \mu m$ was used and S_{back} was set to $1 cms^{-1}$, which represents a passivated back contact.

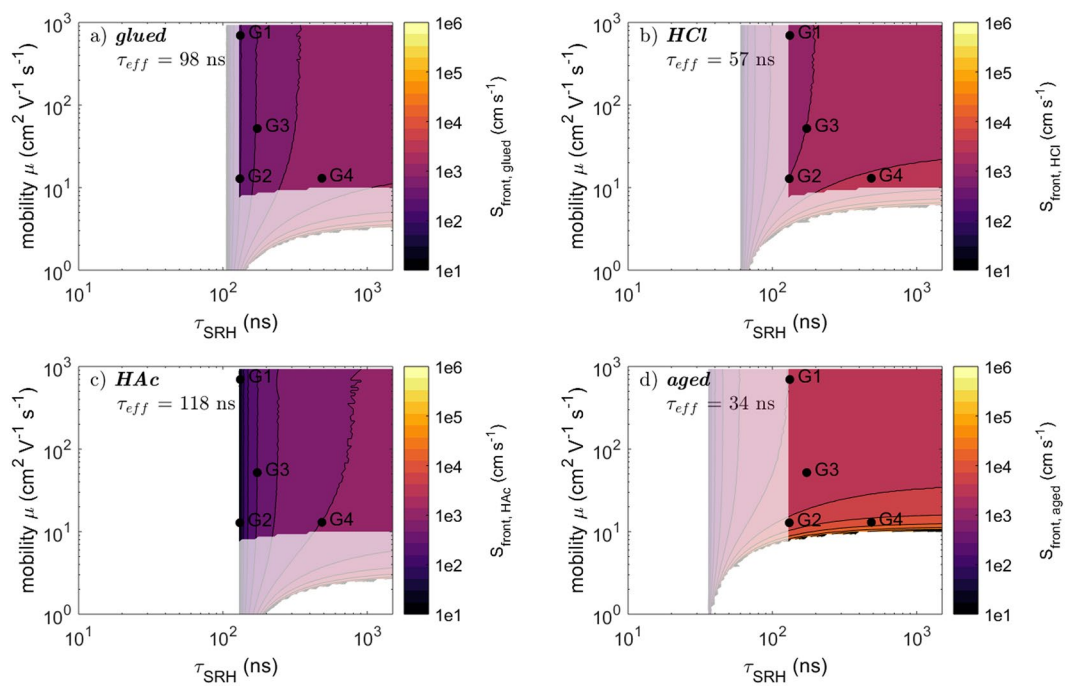


Figure 6. Solutions of the parameters for τ_{bulk} and μ and the surface recombination velocities for the bg-CIGS absorber based on Eqn. (14). The pale areas indicate the solution when taking into account only one decay time for the corresponding sample configuration. Bright areas indicate solutions considering the solutions for all configurations.

Figure 6 shows the valid parameters based on the numerical analysis as similarly carried out for the CIS sample in section 4.1. No map is shown for the *delam* configuration as it is similar to the *glued* case due to similar PL decay times (see Fig. 3b and Table 2). Each map shows the solutions obtained from each individual measurement/configuration (pale areas) as well as the combined solutions (bright areas). The upper and lower bounds are presented in Table 3. The estimates of the surface recombination velocities are comparable to these of the CIS absorber. However, no upper bound of the mobility μ could be identified for the bg-CIGS absorber, which may take large values. In contrast, the mobility in the CIS absorber was quite well confined. The reason for that will be discussed in section 4.3.

Discussion and comparison to simulated transients. Table 3 compiles the boundary values estimated from the mathematical analysis of the decay times, for both CIS and bg-CIGS absorbers. While there is a small difference for $S_{front,glued}$, there is a good match for the two recombination velocities $S_{front,HAc}$ and $S_{front,aged}$. Concerning the bulk properties for the CIS absorber the mobility could be confined between $32\text{--}45\text{ cm}^2\text{ V}^{-1}\text{ s}^{-1}$ and a lower bound of 117 ns for the SRH lifetime τ_{SRH} was determined. It is stressed that this lower bound of τ_{SRH} is much larger than any measured PL decay time demonstrating the influence of surface recombination. For the bg-CIGS absorber only a lower limit of $8.3\text{ cm}^2\text{ V}^{-1}\text{ s}^{-1}$ is identified for the mobility but no upper limit could be deduced. The reason is that for the bg-CIGS absorber no configuration exists with a high enough surface recombination velocity (the back surface is passivated due to the GGI grading). Thus, the parameters (τ_{SRH} , μ , S_{front}) can always be chosen such that the surface recombination rate is limited by the surface recombination velocity and not by the mobility of the charge carriers, which have to diffuse to the recombinative surfaces. Ahrenkiel²² gives approximate analytical expressions for τ_{surf} in the limiting cases of small and high values for $y = \frac{Sd}{D}$ (with $S = S_{front} = S_{back}$ for simplicity). For small values of y (i.e. small surface recombination velocity compared to the mobility) the approximation using $\tan \beta_k d = \beta_k d$ can be applied to Eqn. (7) and it is found²²

$$\tau_{surf} \approx \frac{d}{2S} \quad (15)$$

Clearly, the surface recombination is not dependent on μ , which in turn cannot be confined. In contrast to the bg-CIGS absorber, the CIS absorber exhibits a highly recombinative back contact due to the Mo and the absence of a bandgap gradient. Looking at the decay time and the parameter map in Fig. 4 for the *HAc* configuration, the mobility cannot be increased arbitrarily since for high S_{back} ($S_{back,Mo} = 10^6\text{ cm s}^{-1}$) the surface recombination is mobility limited by diffusion to the recombinative surfaces resulting in²²

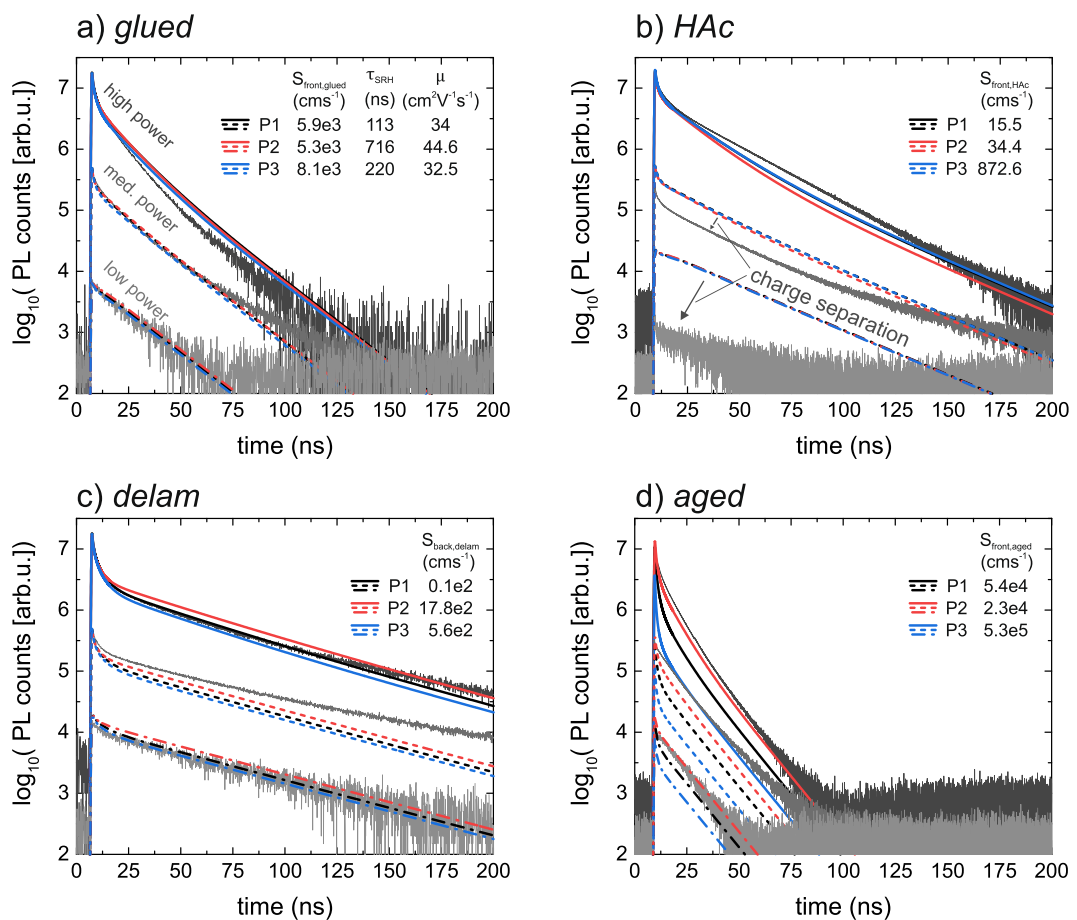


Figure 7. Simulated (colored) and measured (black) transients based on three parameter sets (P1, P2 and P3) deduced by the mathematical considerations in section 4.1. See also Fig. 4 for details of P1, P2 and P3.

$$\tau_{\text{surf}} \approx \frac{d^2}{D^2 \pi^2} \quad (16)$$

These limiting cases show that a measurement with a highly recombinative surface is necessary for confining the mobility towards large values.

An upper limit for the SRH lifetime τ_{SRH} could neither be deduced for the CIS nor for the bg-CIGS absorber, since the parameters can always be chosen in a way that the effective decay time is limited by surface recombination.

Due to the large spread in (valid) parameter values for τ_{SRH} and μ , it cannot be conclusively evaluated if the difference in the measured decay times (bg-CIGS and CIS absorber) is solely due to a passivated back contact for the bg-CIGS absorber, or if also the bulk properties τ_{bulk} and μ are improved for the bg-CIGS device.

Simulation of Transients. In the following, simulated TRPL transients confirm the validity of the mathematical approach, and are used to evaluate if more information can be extracted from the measurements. The transients are simulated using the Matlab script for the parameter sets annotated in Fig. 4 (CIS absorber) and Fig. 6 (bg-CIGS absorber) and are shown in Figs 7,8, respectively. Estimations of the experimentally injected charge carriers are implemented, and the transients are scaled (same factor for all transients) to account for the collection efficiency of the optical system. For all configurations, the injection levels were set to $6.4 \times 10^{10} \text{ cm}^{-2} \text{ pulse}^{-1}$ (low power), $5.3 \times 10^{11} \text{ cm}^{-2} \text{ pulse}^{-1}$ (med. power) and $3.6 \times 10^{12} \text{ cm}^{-2} \text{ pulse}^{-1}$ (high power). Except for the HAc configuration (see discussion below), a good match for the PL yield is found.

By comparison of the simulated transients with the experimental transients at medium power a good match between the decay times (slopes of the transients) between 20 and 80 ns (time range used as input for the mathematical analysis, see Table 2) is observed. Consequently, the mathematical analysis of the decay times is indeed well suited to determine reasonable device parameters. In particular, the approach of defining an effective thickness d_{eff} (for a certain back grading) as described in section 4.2 works reasonably well.

Concerning the transients for the CIS absorber a good match for all injection levels is found for the *glued* (Fig. 7a) and the *delam* (Fig. 7c) configuration; also the initial non-exponential decay is well reproduced. Hence,

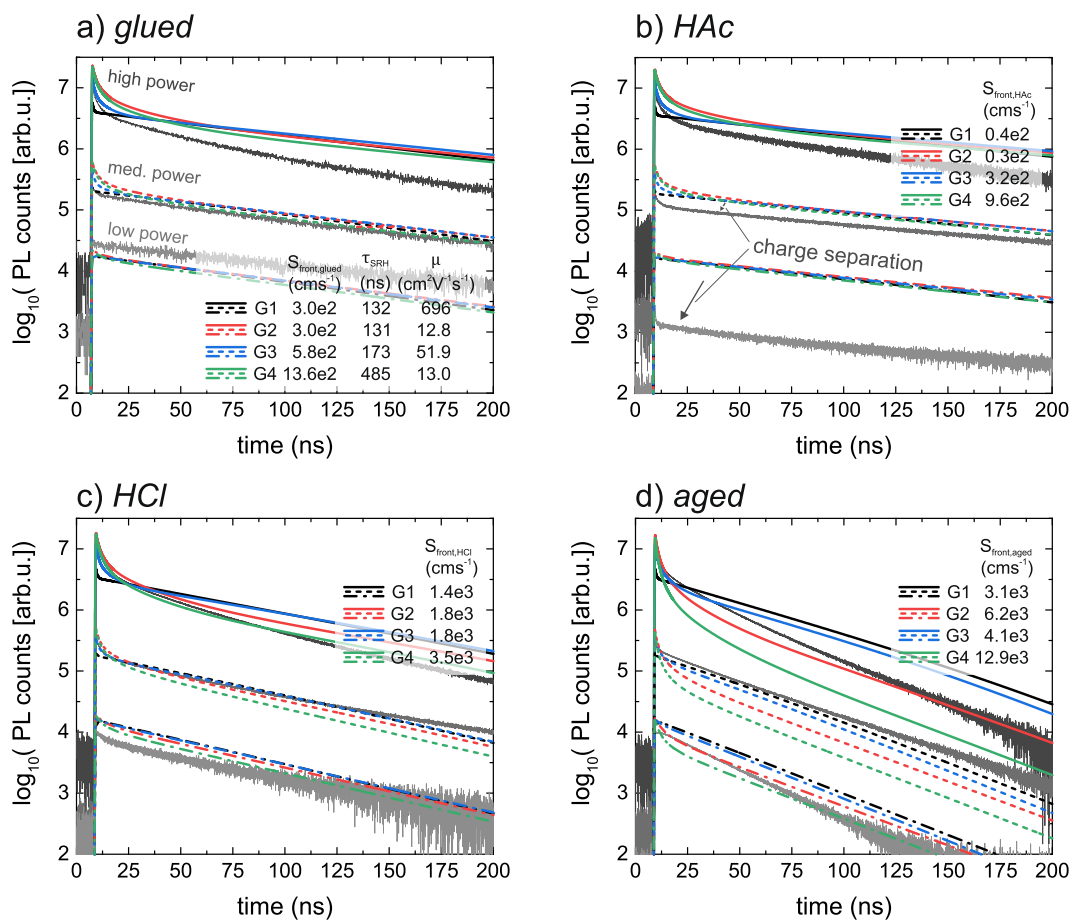


Figure 8. Simulated (colored) and measured (black) transients of the bg-CIGS absorber for the parameter sets G1-G4 as presented in Fig. 6. G1 and G3 are the two sets with rather high mobilities, while G2 and G4 have low μ but span a large range of τ_{SRH} .

no further confinement of τ_{SRH} and μ values can be made by taking additionally the initial decay into account, despite the fact that τ_{SRH} ranges between 117 ns and 716 ns and μ between $32 \text{ cm}^2 \text{V}^{-1} \text{s}^{-1}$ and $45 \text{ cm}^2 \text{V}^{-1} \text{s}^{-1}$ for the simulated transients shown in Fig. 7a,c. In particular, this shows that fitting a transient can become problematic as similar transients are obtained for large deviations of the recombination parameters (in this case only three parameters: S_{front} , μ , τ_{SRH}).

For the HAc configuration the decay times as well as the shape of the initial decay are also well reproduced. However, the experimental maximal PL yield is strongly reduced at low power levels compared to the simulations. This might hint to the fact that the ~50 nm thick CdS layer after the HAc etch introduces a small electric field, which separates the injected charge carriers (already during the pulse) and thus quenches the PL yield³³. The simulated transients for the *aged* configuration deviate slightly and might be explained that the aged surface cannot be solely described by a surface recombination velocity but probably also surface charge needs to be taken into account. Despite that, the parameter set for P3 with a rather high surface recombination velocity of $S_{front,aged} = 5.2 \times 10^5 \text{ cm s}^{-1}$ shows the strongest deviation in the shape of the initial decay and thus might be excluded. Still, this cannot be used to further confine values of τ_{SRH} or μ .

The simulated transients for the bg-CIGS absorber (Fig. 8) can be analyzed similarly. The simulated decays give a good match with the experimental transients for the configurations *glued* (Fig. 8a) and *HCl* (Fig. 8c) except for high power levels, where experimentally a reduced decay time is observed as compared to lower power levels. Also the shape of the initial decay is well reproduced except for the parameter set G1 with $\mu = 696 \text{ cm}^2 \text{V}^{-1} \text{s}^{-1}$. Due to the high mobility the carriers homogenize rather quickly. Consequently, the non-exponential decay caused by bi-molecular recombination and diffusion is observed for considerably shorter times (compared to the other three parameter sets with lower mobilities). Thus, it can be concluded that the mobilities cannot take arbitrarily high values as otherwise the initial decay is not pronounced enough. The initial decay for the parameter set with $\mu = 50 \text{ cm}^2 \text{V}^{-1} \text{s}^{-1}$ still looks reasonable and thus cannot be excluded. To establish a better confinement for the mobility a more detailed analysis for the bg-CIGS absorbers needs to be carried out in terms of the initial decay characteristics, which is however not subject of this paper. The transients for the HAc configuration show a similar behavior as for the CIS absorber, which is a strongly reduced PL yield at low power levels compared to the simulated transients. Again, this might be caused by an electric field present due to the CdS buffer layer. The *aged* transients also deviate slightly as for the CIS case indicating a similar surface modification (i.e. possibly additional surface charges).

It is worth noting that $S_{front, HAc} < S_{front, HCl}$, with $S_{front, HAc} < 1.4 \times 10^3 \text{ cm s}^{-1}$, which shows the passivating effect of the CdS buffer layer. Further, it is worth noting that an electric field potentially caused by the CdS layer (for the HAc configuration) leads to an increased recombination at the front surface due to the attraction of the minority carriers towards the junction. In that case, the upper bound for the real front surface recombination velocity $S_{front, HAc}$ is even lower.

With these simulations we demonstrate that the mathematical approach is an efficient method to systematically explore the large parameter space and provide numerical bounds to recombination parameters. In our case, only marginal information could be gained from the more elaborate transient simulations.

Conclusions

An analysis method is presented to estimate the surface recombination velocities as well as charge carrier mobility and SRH lifetime values based on TRPL measurements. For this purpose, the surface recombination velocities are tuned by applying various surface modifications. This enables to explore systematically the parameter space, to disentangle the contributions of surface and bulk recombination and to determine lower and/or upper bounds of the parameters.

The mathematical analysis was carried out on a CIS and a single back-graded CIGS absorber. Table 3 presents an overview of the bounds for the parameters governing the recombination in these systems. In particular, a surface recombination velocity below $1.4 \times 10^3 \text{ cm s}^{-1}$ was found for the CIS/CdS interface, which is an important parameter for device simulations. For the CIS absorber the mobility was deduced between $32 - 45 \text{ cm}^2 \text{ V}^{-1} \text{ s}^{-1}$. For the bg-CIGS absorber the confinement of mobility values was not as good, as no surface configuration could cause sufficiently large surface recombination to be mobility limited. For the bulk lifetime τ_{SRH} a lower limit of $\tau_{SRH} > 117 \text{ ns}$ was determined for the CIS absorber, indicating relatively good bulk properties even though the highest measured decay time was only 48 ns.

Transients were simulated using a Matlab script with valid sets of device parameters deduced from the mathematical analysis as input. Taking the shape of the initial decay into account, high mobilities around $700 \text{ cm}^2 \text{ V}^{-1} \text{ s}^{-1}$ in the bg-CIGS device could be excluded. However, no further confinement of the bulk lifetimes could be achieved based on the simulations of transients compared to the mathematical model. Nevertheless, a good match of the decay tail times is found showing the validity and effectiveness of the mathematical approach. Even for a large range of parameters, the initial decay is generally well reproduced, demonstrating that fitting procedures for the determination of the recombination parameters is problematic. In case of a fitting procedure it is thus recommended to use various excitation wavelengths to vary the shape of the initial decay as for instance applied in¹⁷.

Data Availability

The datasets generated during and/or analyzed during the current study are available from the corresponding author on reasonable request.

References

1. Repins, I. L. *et al.* Fiber-fed time-resolved photoluminescence for reduced process feedback time on thin-film photovoltaics. *Review of Scientific Instruments* **86**, <https://doi.org/10.1063/1.4905535> (2015).
2. Chantana, J. *et al.* Investigation of Cu(In,Ga)Se₂ absorber by time-resolved photoluminescence for improvement of its photovoltaic performance. *Solar Energy Materials and Solar Cells* **130**, 567–572, <https://doi.org/10.1016/j.solmat.2014.08.012> (2014).
3. Repins, I. L., Metzger, W. K., Perkins, C. L., Li, J. V. & Contreras, M. A. In *Conference Record of the IEEE Photovoltaic Specialists Conference*. 000978–000983.
4. Ohnesorge, B. *et al.* Minority-carrier lifetime and efficiency of Cu(In,Ga)Se₂ solar cells. *Applied Physics Letters* **73**, 1224–1226, <https://doi.org/10.1063/1.1221134> (1998).
5. Metzger, W. K. *et al.* Recombination kinetics and stability in polycrystalline Cu(In,Ga)Se₂ solar cells. *Thin Solid Films* **517**, 2360–2364, <https://doi.org/10.1016/j.tsf.2008.11.050> (2009).
6. Kephart, J. M. *et al.* Sputter-Deposited Oxides for Interface Passivation of CdTe Photovoltaics. *IEEE Journal of Photovoltaics*, <https://doi.org/10.1109/JPHOTOV.2017.2787021> (2018).
7. Staub, F. *et al.* Beyond Bulk Lifetimes: Insights into Lead Halide Perovskite Films from Time-Resolved Photoluminescence. *Physical Review Applied* **6**, <https://doi.org/10.1103/PhysRevApplied.6.044017> (2016).
8. Wu, B. *et al.* Discerning the Surface and Bulk Recombination Kinetics of Organic–Inorganic Halide Perovskite Single Crystals. *Advanced Energy Materials* **6**, <https://doi.org/10.1002/aenm.201600551> (2016).
9. Stranks, S. D. *et al.* Electron–hole diffusion lengths exceeding 1 micrometer in an organometal trihalide perovskite absorber. *Science* **342**, 341–344, <https://doi.org/10.1126/science.1243982> (2013).
10. Xing, G. *et al.* Long-range balanced electron-and hole-transport lengths in organic-inorganic CH₃NH₃PbI₃. *Science* **342**, 344–347, <https://doi.org/10.1126/science.1243167> (2013).
11. Otaredian, T. Separate contactless measurement of the bulk lifetime and the surface recombination velocity by the harmonic optical generation of the excess carriers. *Solid State Electronics* **36**, 153–162, [https://doi.org/10.1016/0038-1101\(93\)90134-C](https://doi.org/10.1016/0038-1101(93)90134-C) (1993).
12. Yang, Y. *et al.* Low surface recombination velocity in solution-grown CH₃NH₃PbBr₃ perovskite single crystal. *Nature Communications* **6**, <https://doi.org/10.1038/ncomms8961> (2015).
13. Metzger, W. K. *et al.* Recombination kinetics and stability in polycrystalline Cu(In,Ga)Se₂ solar cells. *Thin Solid Films* **517**, 2360–2364, <https://doi.org/10.1016/j.tsf.2008.11.050> (2009).
14. Barnard, E. S. *et al.* Probing carrier lifetimes in photovoltaic materials using subsurface two-photon microscopy. *Scientific Reports* **3**, <https://doi.org/10.1038/srep02098> (2013).
15. Kuciauskas, D. *et al.* Minority carrier lifetime analysis in the bulk of thin-film absorbers using subbandgap (Two-Photon) excitation. *IEEE Journal of Photovoltaics* **3**, 1319–1324, <https://doi.org/10.1109/JPHOTOV.2013.2270354> (2013).
16. Ahrenkiel, R. K. & Johnston, S. W. An optical technique for measuring surface recombination velocity. *Solar Energy Materials and Solar Cells* **93**, 645–649, <https://doi.org/10.1016/j.solmat.2008.12.028> (2009).
17. Hempel, H., Hages, C. J., Eichberger, R., Repins, I. & Unold, T. Minority and Majority Charge Carrier Mobility in Cu₂ZnSnSe₄ revealed by Terahertz Spectroscopy. *Scientific Reports* **8**, <https://doi.org/10.1038/s41598-018-32695-6> (2018).
18. Feurer, T. *et al.* Single-graded CIGS with narrow bandgap for tandem solar cells. *Science and Technology of Advanced Materials* **19**, 263–270, <https://doi.org/10.1080/14686996.2018.1444317> (2018).

19. Sze, S. & Ng, K. K. *Physics of Semiconductor Devices: Third Edition*. (2006).
20. Maiberg, M. & Scheer, R. Theoretical study of time-resolved luminescence in semiconductors. I. Decay from the steady state. *Journal of Applied Physics* 116, <https://doi.org/10.1063/1.4896483> (2014).
21. Abou-Ras, D., Kirchartz, T. & Rau, U. *Advanced Characterization Techniques for Thin Film Solar Cells*. (2011).
22. Ahrenkiel, R. K. In *Semiconductors and Semimetals* Vol. 39 39–150 (1993).
23. Maiberg, M. & Scheer, R. Theoretical study of time-resolved luminescence in semiconductors. II. Pulsed excitation. *Journal of Applied Physics* 116, <https://doi.org/10.1063/1.4896484> (2014).
24. Sproul, A. B. Dimensionless solution of the equation describing the effect of surface recombination on carrier decay in semiconductors. *Journal of Applied Physics* 76, 2851–2854, <https://doi.org/10.1063/1.357521> (1994).
25. Maiberg, M., Hölscher, T., Zahedi-Azad, S., Fränzel, W. & Scheer, R. Investigation of long lifetimes in Cu(In,Ga)Se₂ by time-resolved photoluminescence. *Applied Physics Letters* 107, <https://doi.org/10.1063/1.4931632> (2015).
26. Maiberg, M., Hölscher, T., Zahedi-Azad, S. & Scheer, R. Theoretical study of time-resolved luminescence in semiconductors. III. Trap states in the band gap. *Journal of Applied Physics* 118, <https://doi.org/10.1063/1.4929877> (2015).
27. López Salas, J. F. *et al.* Simulation of metastable changes in time resolved photoluminescence of Cu(In,Ga)Se₂ thin film solar cells upon light soaking treatment. *Thin Solid Films* 633, 40–44 (2017).
28. Redinger, A. *et al.* Time resolved photoluminescence on Cu(In, Ga)Se₂ absorbers: Distinguishing degradation and trap states. *Applied Physics Letters* 110, <https://doi.org/10.1063/1.4977707> (2017).
29. Carron, R. *et al.* Refractive indices of layers and optical simulations of Cu(In,Ga)Se₂ solar cells. *Science and Technology of Advanced Materials* 19, 396–410, <https://doi.org/10.1080/14686996.2018.1458579> (2018).
30. Metzger, W. K., Ahrenkiel, R. K., Dashdorj, J. & Friedman, D. J. Analysis of charge separation dynamics in a semiconductor junction. *Physical Review B - Condensed Matter and Materials Physics* 71, <https://doi.org/10.1103/PhysRevB.71.035301> (2005).
31. Regesch, D. *et al.* Degradation and passivation of CuInSe₂. *Applied Physics Letters* 101 (2012).
32. Metzger, W. K., Repins, I. L. & Contreras, M. A. Long lifetimes in high-efficiency Cu(In,Ga)Se₂ solar cells. *Applied Physics Letters* 93, 022110 (2008).
33. Heise, S. J. & López Salas, J. F. Charge separation effects in time-resolved photoluminescence of Cu(In,Ga)Se₂ thin film solar cells. *Thin Solid Films* 633, 35–39, <https://doi.org/10.1016/j.tsf.2016.11.031> (2017).

Acknowledgements

This work received financial support partially by the Swiss State Secretary for Education, Research and Innovation (SERI) under contract number 15.0158 (Horizon2020 project Sharc25) and under contract number 17.00105 (EMPIR project HyMet) and by the Swiss National Science Foundation (SNSF) under contract number 407040_153952 (NRP 70 “Energy Turnaround” project PV2050).

Author Contributions

Thomas Paul Weiss and Benjamin Bissig contributed equally in analyzing and measuring the TRPL data. Thomas Paul Weiss prepared the manuscript. Benjamin Bissig wrote the Matlab code for the TRPL solver. Thomas Feurer grew the samples under investigation. Romain Carron helped in the analysis and discussion and prepared Figure 4 and Figure 6. Stephan Buecheler and Ayodhya N. Tiwari supervised the work. All authors reviewed the manuscript.

Additional Information

Supplementary information accompanies this paper at <https://doi.org/10.1038/s41598-019-41716-x>.

Competing Interests: The authors declare no competing interests.

Publisher's note: Springer Nature remains neutral with regard to jurisdictional claims in published maps and institutional affiliations.



Open Access This article is licensed under a Creative Commons Attribution 4.0 International License, which permits use, sharing, adaptation, distribution and reproduction in any medium or format, as long as you give appropriate credit to the original author(s) and the source, provide a link to the Creative Commons license, and indicate if changes were made. The images or other third party material in this article are included in the article's Creative Commons license, unless indicated otherwise in a credit line to the material. If material is not included in the article's Creative Commons license and your intended use is not permitted by statutory regulation or exceeds the permitted use, you will need to obtain permission directly from the copyright holder. To view a copy of this license, visit <http://creativecommons.org/licenses/by/4.0/>.

© The Author(s) 2019